RSC Advances

ROYAL SOCIETY OF CHEMISTRY

PAPER

View Article Online
View Journal | View Issue

Cite this: *RSC Adv.*, 2024, **14**, 5193

Fabrication of highly stretchable salt and solvent blended PEDOT:PSS/PVA free-standing films: non-linear to linear electrical conduction response†

Sanjib Sau and Sarathi Kundu *

Nowadays, ductile and conducting polymeric materials are highly utilizable in the realm of stretchable organic electronics. Here, mechanically ductile and electrically conducting free-standing films are fabricated by blending different solvents such as dimethyl sulfoxide (DMSO), diethylene glycol (DEG) and *N*,*N*-dimethylformamide (DMF), and salts such as silver nitrate ($AgNO_3$), zinc chloride ($ZnCl_2$), copper chloride ($CuCl_2$) and indium chloride ($InCl_3$) with the homogeneous solution of poly(3,4-ethylenedioxythiophene):polystyrenesulfonate (PEDOT:PSS) and poly(vinyl alcohol) (PVA) through solution casting method. The presence of salt modifies the PEDOT conformation from benzoid to quinoid, and induces the evolution of different morphologies. $ZnCl_2$ or $AgNO_3$ blended films have lower surface roughness and good miscibility with polymers, while $CuCl_2$ or $InCl_3$ blended films have relatively higher surface roughness as well as irregularly distributed surface morphology. Some crystalline domains are also formed due to the salt agglomeration. The presence of salt inside PEDOT:PSS/PVA/solvent system changes the current–voltage response from non-linear to linear. Among all the films, zinc salt blended PEDOT:PSS/PVA/DMSO, PEDOT:PSS/PVA/DEG and PEDOT:PSS/PVA/DMF films have higher conductivity, and zinc salt blended PEDOT:PSS/PVA/DEG film shows the highest conductivity of 0.041 ± 0.0014 S cm^{-1}, while silver salt blended PEDOT:PSS/PVA/DMSO, PEDOT:PSS/PVA/DEG and PEDOT:PSS/PVA/DMF films have higher elongation at break, and silver salt blended PEDOT:PSS/PVA/DMSO film shows the highest elongation at break of 670 ± 31%. Both the charge carriers, *i.e.*, electrons and ions, contribute to the electrical conduction, and the presence of hydrogen bonds and ionic interactions among $PEDOT^+$, PSS^-, PVA, residual solvent, salt cations and anions modifies the film behaviours. Among all the films, $ZnCl_2$ blended PEDOT:PSS/PVA/DMSO film offers relatively superior behaviours having higher conductivity (0.025 ± 0.0013 S cm^{-1}) and elongation at break (517 ± 15%), and therefore can have potential applications in the fields of wearable devices, bioelectronics, *etc.*

Received 4th December 2023
Accepted 2nd February 2024

DOI: 10.1039/d3ra08260a

rsc.li/rsc-advances

1. Introduction

Intrinsically conducting polymers (ICPs) have been significantly used in the realm of organic electronics since the invention of highly conducting polyacetylene in the 1970s.[1,2] They have alternate single and double bonds in the conjugated backbone and as a result localized and delocalized states are formed inside the ICPs. The delocalized π bonds generate charge carriers such as solitons, polarons, bipolarons, *etc.* and therefore, exhibit high conductivity as well as interesting optical properties.[3–5] However, a rigid conjugated backbone and strong interaction between cations and anions make ICPs as glassy-like state and mechanically brittle materials at room temperature.[6] Some of the well-known ICPs are polypyrrole (PPy), polythiophene (PTH), polyacetylene (PA), polyaniline (PANI), *etc.*[4,7] Though these conducting polymers exhibit satisfactory performance, still they are not utilized extensively in the fields of different applications owing to their high cost and temperature sensitiveness, and for not having practically desirable electrical and mechanical performances.[8] For achieving fruitful properties, derivatives of ICPs are prepared through modification or polymerization of conductive polymers. One common example is poly(3,4-ethylenedioxythiophene) (PEDOT), which is a derivative of polythiophene. PEDOT is usually derived by polymerization of EDOT monomers through electrochemical method, emulsion polymerization method and chemical oxidation synthesis method.[2,9–11] Though intrinsic PEDOT (positively charged) has good conductivity as well as good stability, but it faces difficulty to dissolve in organic solvents or water. To overcome this problem, PEDOT is generally blended with hydrophilic and insulating negatively charged polystyrene sulfonic acid (PSS) to obtain

Soft Nano Laboratory, Physical Sciences Division, Institute of Advanced Study in Science and Technology, Vigyan Path, Paschim Boragaon, Garchuk, Guwahati, Assam 781035, India. E-mail: sarathi.kundu@gmail.com

† Electronic supplementary information (ESI) available. See DOI: https://doi.org/10.1039/d3ra08260a

poly(3,4-ethylenedioxythiophene):polystyrenesulfonate (PEDOT:PSS) in aqueous solution.[12–14] PEDOT:PSS shows outstanding properties such as transparent in the visible region, water soluble, thermally stable, capable of film forming and tuneable electrical and mechanical properties. It is enormously applied in the diverse fields such as organic electrodes, light emitting diodes, solar cells, field-effect transistors, photovoltaics (PVs), and different electronic sensors, *e.g.*, strain sensor, pressure sensor, temperature sensor, humidity sensor and biosensor.[15–18] PEDOT:PSS has high Young's modulus and low ductility. Though PEDOT:PSS has high conductivity, but due to its brittleness, *i.e.*, low viscosity, it is unable to form free-standing film and hence, it loses its applications in the fields of flexible and stretchable electronics.[19–22]

To use PEDOT:PSS in flexible and stretchable electronics, different approaches have been taken, *e.g.*, blending of PEDOT:PSS with additives, preparation of PEDOT:PSS nanofibers or nanowires, deposition of PEDOT:PSS on elastomers or encapsulating materials, *etc.*[19] Some water soluble elastomers such as poly(vinyl alcohol) (PVA), polyurethane (PU), poly(-dimethylsiloxane) (PDMS), *etc.* are blended with PEDOT:PSS for the processing of mechanically flexible and stretchable free-standing films.[7,21,23,24] PVA is a synthetic polymer which is extensively utilized for this purpose due to its superior properties like high water solubility, good free standing film forming capability, biocompatibility, biodegradability, efficient mechanical response and low cost.[25–28] However, PEDOT:PSS/elastomer does not have true reversible mechanical properties owing to the poor elasticity of these elastomers and also these insulating elastomers significantly lower the conductivity of PEDOT:PSS/elastomer compared to pristine PEDOT:PSS due to the hindrance of connectivity between PEDOT chains.[19] To solve these drawbacks, some secondary dopants such as polar organic solvents (*e.g.* dimethyl sulfoxide (DMSO), methanol, ethylene glycol (EG), diethylene glycol (DEG), tetrahydrofuran (THF), *N*,*N*-dimethylformamide (DMF), sorbitol, *etc.*), salts (*e.g.* $NaClO_4$, $CuCl_2$, NaCl, NH_4Cl, *etc.*), ionic liquids, surfactants (*e.g.* Triton X-100 and Zonyl-FS300), ionic liquids, acids, bases and zwitterions are blended, or pre- and post-treated with PEDOT:PSS/elastomer. These secondary dopants act as plasticizers, which can enhance electrical conductivity and ductility significantly by weakening the interaction between PEDOT and PSS chains leading to increase in free volume.[16,19,22,29–31]

There are several reports on stretchable conducting free-standing films. He *et al.* reported salt-induced ductilization where free-standing PEDOT:PSS film was post treated by different chemical agents such as EG, formic acid (FA) and methanesulfuric acid (MSA) followed by another post treatment by various salts such as sodium perchlorate ($NaClO_4$), sodium chloride (NaCl), ammonium chloride (NH_4Cl) and copper(II) chloride ($CuCl_2$). It was observed that EG/PEDOT:PSS film post treated with $NaClO_4$ salt showed maximum enhancement of elongation at break which was around 53.2%, whereas EG/PEDOT:PSS film had below 10%. These ductilized PEDOT:PSS films had almost strain-insensitive resistance.[6] Yang *et al.* prepared conductive elastomer by blending PEDOT:PSS with natural rubber (NR). 10 wt% PEDOT:PSS/NR blended film doped with DMSO exhibited the conductivity value of around 87 S cm^{-1} and the elongation at break of around 490%. It showed self-powered temperature and tensile strain-sensing property.[19] Gong *et al.* made flexible and stretchable conductive and strain-sensitive hydrogel by mixing PVA and PEDOT:PSS with reinforcing agent sodium polyacrylate (PAANa). Due to PAANa doping, tensile strength was improved, and also elongation at break and conductivity were enhanced from 254% to 289%, and 0.054 S m^{-1} to 0.146 S m^{-1} respectively. Apart from that, treatment by saturated NaCl salt solution also enhanced the tensile strength, elongation at break and electrical conductivity to 1.97 MPa, 380% and 0.327 S m^{-1} respectively.[32] Gao *et al.* reported flexible and conducting fibre of PEDOT:PSS/PVA/EG as a wearable sensor. They found that PEDOT:PSS/20 wt% PVA/10 wt% EG exhibited the optimal tensile strength and elongation at break as 210 ± 5 MPa and 26 ± 1.5% respectively.[33] Xia *et al.* observed charge screening conductivity enhancement of PEDOT:PSS films by treating various salts such as copper(II) chloride ($CuCl_2$), indium chloride ($InCl_3$), sodium chloride (NaCl), magnesium chloride ($MgCl_2$), silver nitrate ($AgNO_3$), lithium chloride (LiCl) and nickel chloride ($NiCl_2$). They observed several times higher conductivity enhancement for 0.74 M $CuCl_2$ solution compared to pristine PEDOT:PSS film.[34]

In this article, we have prepared PEDOT:PSS/PVA flexible and stretchable conducting films in presence of different solvents (DMSO, DEG and DMF) and salts ($AgNO_3$, $ZnCl_2$, $CuCl_2$ and $InCl_3$). The conductivity enhancement of PEDOT:PSS blended film depends upon the softness parameter of the metal ions. Owing to the positive softness parameters of Ag^+, Zn^{2+}, Cu^{2+} and In^{3+} cations, the above chosen salts may significantly increase the conductivity of the as prepared film. Salts also act as plasticizers which can enhance the ductility of the as prepared composite films.[34–36] Therefore, the effect of cations having positive softness parameters can provide superior electrical and mechanical properties of PEDOT:PSS/PVA films for its practical applications. We believe that the results as obtained from the current work and the proposed mechanism will be useful for novel applications.

2. Experimental details

2.1. Materials

Poly(vinyl alcohol) (PVA) (cat. no. 8.43866.1000, M.W. = 60 000 g mol^{-1} and 99% purity) was supplied by Merck. 1.3 wt% PEDOT:PSS dispersed in water (cat. no. 483095) and silver paste (cat. no. 735825) were purchased from Sigma-Aldrich. DMSO (Sigma-Aldrich, cat. no. 472301-1L, M.W. = 78.13 g mol^{-1} and density ≈ 1.10 g mL^{-1}), DEG (Merck, cat. no. 80313105001046, M.W. = 106.12 g mol^{-1} and density ≈ 1.12 g mL^{-1}) and *N*,*N*-dimethylformamide (DMF) (Merck, cat. no. 8.22275.0521, M.W. = 73.09 g mol^{-1} and density ≈ 0.94 g mL^{-1}) were procured and used. Silver nitrate ($AgNO_3$, Merck, cat. no. 1.93200.0027, M.W. = 169.87 g mol^{-1} and assay ≥ 99.5%), zinc chloride ($ZnCl_2$, Merck, cat. no. 1.93623.0521, M.W. = 136.30 g mol^{-1} and assay ≥ 95%), copper(II) chloride dihydrate ($CuCl_2 \cdot 2H_2O$, Merck, cat. no.

1.93691.0521, M.W. = 170.48 g mol^{-1} and assay ≥ 98.5%) and indium(III) chloride ($InCl_3$, Sigma-Aldrich, cat. no. 429414-5G, M.W. = 221.18 g mol^{-1} and assay 99.99%) were purchased and utilized. Fig. 1(a)–(e) represent chemical structures of PEDOT:PSS, PVA, DMSO, DEG and DMF respectively. Double-distilled water (resistivity ≈ 18.2 MΩ cm, Millipore Milli-Q system) was used for the entire experimental purpose.

2.2. Fabrication of films

In the previous studies, we prepared PEDOT:PSS/PVA film as well as solvents (DMSO, DEG and DMF) blended PEDOT:PSS/PVA free-standing films by solution casting method and their properties were studied.[37,38] In this work, all the free-standing films were prepared by blending PVA, PEDOT:PSS, solvent and salt followed by solution casting method. At first, PVA was stirred at around 3 h at 80 °C in the double-distilled water for getting homogeneously dissolved PVA. Next, $AgNO_3$ was added into the homogeneous PVA solution followed by 30 min stirring at 80 °C. After that, PEDOT:PSS was poured into the solution followed by 30 min stirring at 80 °C. At last, DMSO was added into the solution followed by 30 min stirring at 80 °C. Prepared solution was casted on polystyrene Petri dish and dried for 72 h at room temperature to get free standing film. Like $AgNO_3$, free standing films were also prepared using other salts like $ZnCl_2$, $CuCl_2$ and $InCl_3$. In the similar way, films were prepared using DEG and DMF and also for each solvent, $AgNO_3$, $ZnCl_2$, $CuCl_2$ and $InCl_3$ were used. In the final solution, concentrations of PVA and PEDOT:PSS were 5 and 0.5 wt% respectively, which are similar to our previous works.[37,38] In this work, concentrations of DMSO, DEG and DMF were chosen as 7, 3 and 10 wt% respectively owing to the optimum electrical responses at these concentrations as obtained from our previous works[37,38] and concentration of each salt was 5 wt%. For all the graphs and also in subsequent sections, PEDOT:PSS/PVA film is designated as PP-P while PEDOT:PSS/PVA/DMSO, PEDOT:PSS/PVA/DEG and PEDOT:PSS/PVA/DMF films are designated as DO, DG and DF respectively. PEDOT:PSS/PVA/DMSO/salt films are designated as DO-Ag, DO-Zn, DO-Cu and DO-In, whereas PEDOT:PSS/PVA/DEG/salt films are designated as DG-Ag, DG-Zn, DG-Cu and DG-In, and PEDOT:PSS/PVA/DMF/salt films are designated as DF-Ag, DF-Zn, DF-Cu and DF-In respectively. Fig. 1(f) represents the formation of film after drying the casted solution on Petri dish. Fig. 1(g) depicts the electrically conducting nature of the as prepared film. Film flexibility is shown in Fig. 1(h), whereas left and right images of Fig. 1(i) indicate the stretchable nature during tensile testing for DO-Ag and DF-Cu films respectively.

2.3. Characterization techniques

The experiments related to X-ray diffraction were performed using D8 Advanced, Bruker, AXS X-ray diffractometer (XRD), where Cu sealed-tube source was used. XRD was operated at 40 kV (voltage) and 40 mA (current). For the selection and enhancement of Cu K_α radiation ($\lambda = 1.54$ Å), Göbel mirror was utilized and the scattered beam was collected by a NaI scintillation (point) detector. X-ray data was taken at 1° min^{-1} (scan speed) and 5–60° (angular range (2θ)). Thermal experiments, *i.e.*, thermogravimetric analyses (TGA) in a nitrogen atmosphere

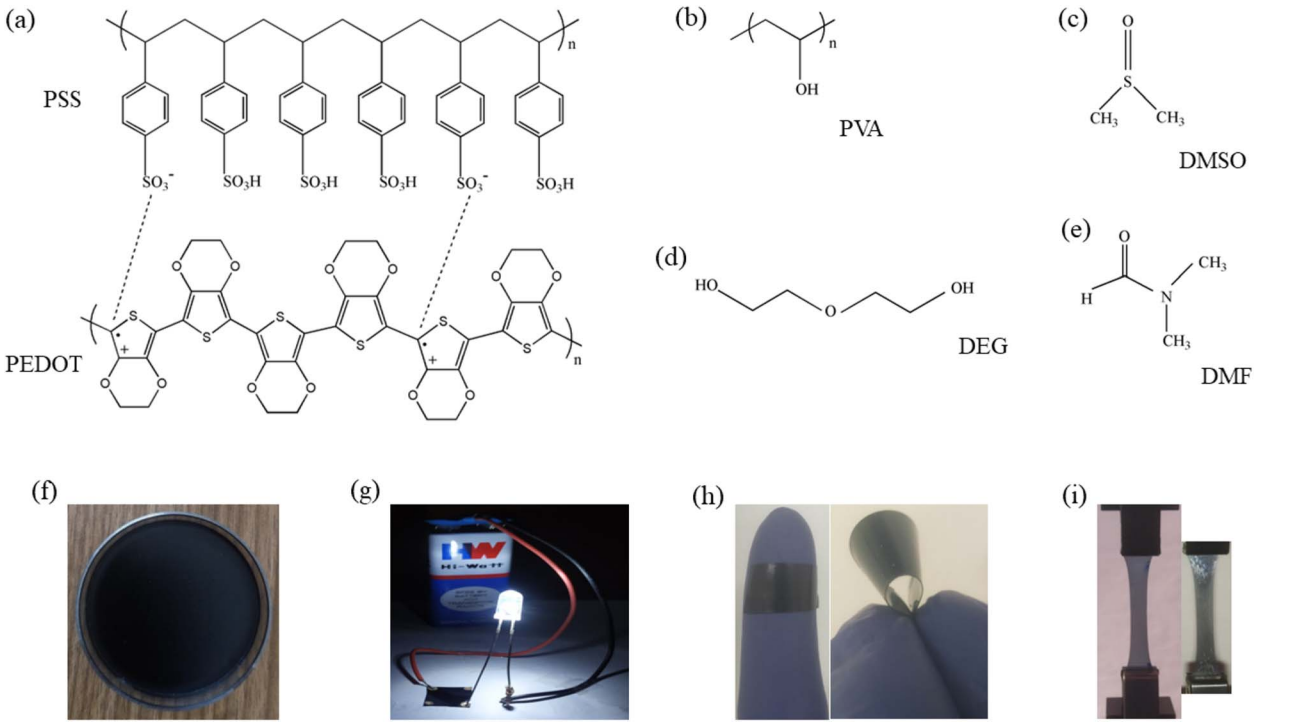

Fig. 1 (a–e) Chemical structures of PEDOT:PSS, PVA, DMSO, DEG and DMF respectively, (f) air dried composite film, (g) LED bulb glowing connecting through the film, (h) flexible nature of the film and (i) DO-Ag (left) and DF-Cu (right) films during tensile experiment.

maintaining the heating rate at 10 °C min^{-1} were performed using TGA 4000, PerkinElmer. Fourier transform infrared (FTIR) measurements (ATR mode) in the range of 600–4000 cm^{-1} over 10 scans were performed using PerkinElmer FTIR spectrophotometer. Raman spectra were taken from Lab-Ram HR evolution (Horiba scientific), where 532 nm laser source was used and exposure time was 4 s. UV-visible absorption results were collected from Shimadzu UV-1800 spectrometer. The surface morphology images were captured from Atomic Force Microscope (AFM) (NTEGRA Prima, NT-MDT Technology, in semi-contact mode using silicon cantilever) and also from Field Emission Scanning Electron Microscope (FESEM) (SIGMA 300, ZEISS). Film thickness measurements were done using Mitutoyo Digimatic Micrometer. Mechanical tests were performed at deformation rate of 3 mm min^{-1} through ASTM D638-10 method from H5KL, Tinius Olsen. For mechanical test, sample gage length and width were kept as 10 and 8 mm respectively. All the mechanical parameters were calculated taking average over five individual film samples for each type. Loading–unloading cycles were collected for twenty successive cycles for each type of the film. In-plane DC electrical measurements were carried out through Keithley 2635B source meter on 10 × 10 mm^2 sample, whereas silver paste was pasted at four corners of the sample for making the electrodes. DC results were collected for eight times from each film changing the voltage and current terminals.

3. Results and discussion

3.1. Thermogravimetric analysis (TGA)

TGA thermograms are collected and presented in Fig. S1 (ESI†) to obtain the thermal stability and thermal degradation steps of the prepared films and to confirm whether DMSO, DEG and DMF are present inside the films or not. DMSO, DEG and DMF have boiling temperatures of ≈189, 244 and 153 °C respectively and, densities and dielectric constants of ≈1.10, 1.12 and 0.94 g mL^{-1}, and ≈46.7, 37 and 36.7 respectively.[39] Due to 72 h drying at room temperature, large fractions of DMSO, DEG and DMF molecules are evaporated but still some residual molecules may reside inside the films due to their low vapour pressures, *i.e.*, low volatility (≈55.6, 0.8 and 516 Pa at room temperature respectively). All the films exhibit six stages of weight loss. First stage of weight loss becomes prominent from 35 to 110 °C, which ascribes to the removal of moisture.[10] In this region, DO-Cu and DO-In films show slow weight loss compared to other films indicating less physically adsorbed water by DO-Cu and DO-In films. Second stage of weight loss is observed in the ranges of 111–188.2 °C, 133–264 °C, 140–174 °C, 144–216 °C, 110–183.1 °C and 110–162.7 °C for DO-Ag, DO-Zn, DO-Cu, DO-In, DG-Ag and DG-Cu films respectively. This weight loss indicates the presence of DMSO and DEG in the films.[38,40,41] For the similar films, third stage of weight loss is evident in between 188.2–203 °C, 264–319 °C, 174–338 °C, 216–248 °C, 183.1–231.9 °C and 162.7–331 °C respectively owing to the degradation of side chains of PVA and PSS.[24,32] Fourth stage of weight loss becomes evidenced in between 257–445 °C, 319–386 °C, 338–431 °C, 248–292 °C, 231.9–481 °C and 331–404 °C respectively representing the removal of Cl and also NO_3 as nitrous oxide (N_2O) and nitric oxide (NO) from the samples.[42,43] At the fifth stage, weight loss is found in the ranges of 470–517 °C, 386–614 °C, 431–763 °C, 292–421 °C, 481–534 °C and 404–670 °C respectively, as decomposition of carbon skeleton or backbone of PEDOT, PSS and PVA occurs.[10,44] Beyond fifth weight loss region, there is a little weight loss which might be occurred owing to other thermal pyrolysis processes.[32] At last, huge percentage of weight remain as ashes mainly attributing to yield elements like Ag, Zn, Cu and In, and their oxides. It is found that after first stage of weight loss, DO-Ag and DG-Ag films have lower thermal stability compared to the other films, whereas DO-In shows highest thermal stability throughout the entire temperature region. Here it is better to mention that some DMSO and DEG molecules are present inside the films. DMF also exists for such type of films, which was reported in our previous work.[38] It is vivid that Ag, Zn, Cu and In salts mixed PEDOT:PSS/PVA films have different temperature regions for six different weight loss stages, which may depend on the interactions between different components.[45,46]

3.2. UV-visible absorption spectra

UV-vis absorption spectra as exhibited in Fig. 2(a), are collected for the determination of optical properties of the prepared composite films. Our previous work showed two absorption peaks at 280 and 330 nm for pure PVA film, which attribute to the bonding (π) to antibonding (π*) transition and non-bonding (n) to antibonding (π*) transition respectively causing from the resonating carbonyl group (>C═O) existing in the PVA chains.[46] In another work, one absorption peak for PP-P film is found at 261 nm (π–n transition) attributing to PSS (aromatic rings) in PEDOT:PSS, another two peaks at 290 and 359 nm as PVA absorptions are red-shifted due to the interaction *via* hydrogen bonding between PSS and PVA, and one another absorption peak at 844 nm due to PEDOT.[38,39,47] Here, it is obvious that DO-Ag, DG-Ag and DF-Ag films exhibit absorption peaks at around 270 (shifted PSS), 311 (Ag^+ ions) and 374 (shifted PVA) nm respectively.[43,46] DO-Zn film exhibits absorption peaks at around 263 (shifted PSS), 367 (shifted PVA) and 863 (shifted PEDOT) nm. DO-Cu film has three absorption peaks at around 262 (shifted PSS), 359 (shifted PVA) and 846 (shifted PEDOT) nm. DO-In film shows absorption peaks at around 262 (shifted PSS), 363 (shifted PVA) and 852 (shifted PEDOT) nm. The presence of salt and solvent makes red-shifting of PSS peak from 261 nm. Apart from that, salt and solvent induce red-shifting of PVA and PEDOT peaks from 330 and 844 nm respectively. The peak-shifting vindicates the interactions among different components, *i.e.*, attractive interaction between salt cations and PSS^-, attractive interaction between salt anions and $PEDOT^+$, interaction between salt cations and PVA, hydrogen bonding between PVA and PSS, and hydrogen bonding of residual solvent with PVA and PSS.[31,34,37,38,43,45,46] Therefore, it lowers the intra- and inter-molecular hydrogen bonding between PVA molecules. At the same time, the ion-exchanged mechanism between PEDOT:PSS and salt ions promotes decoupling of PEDOT from PSS, which

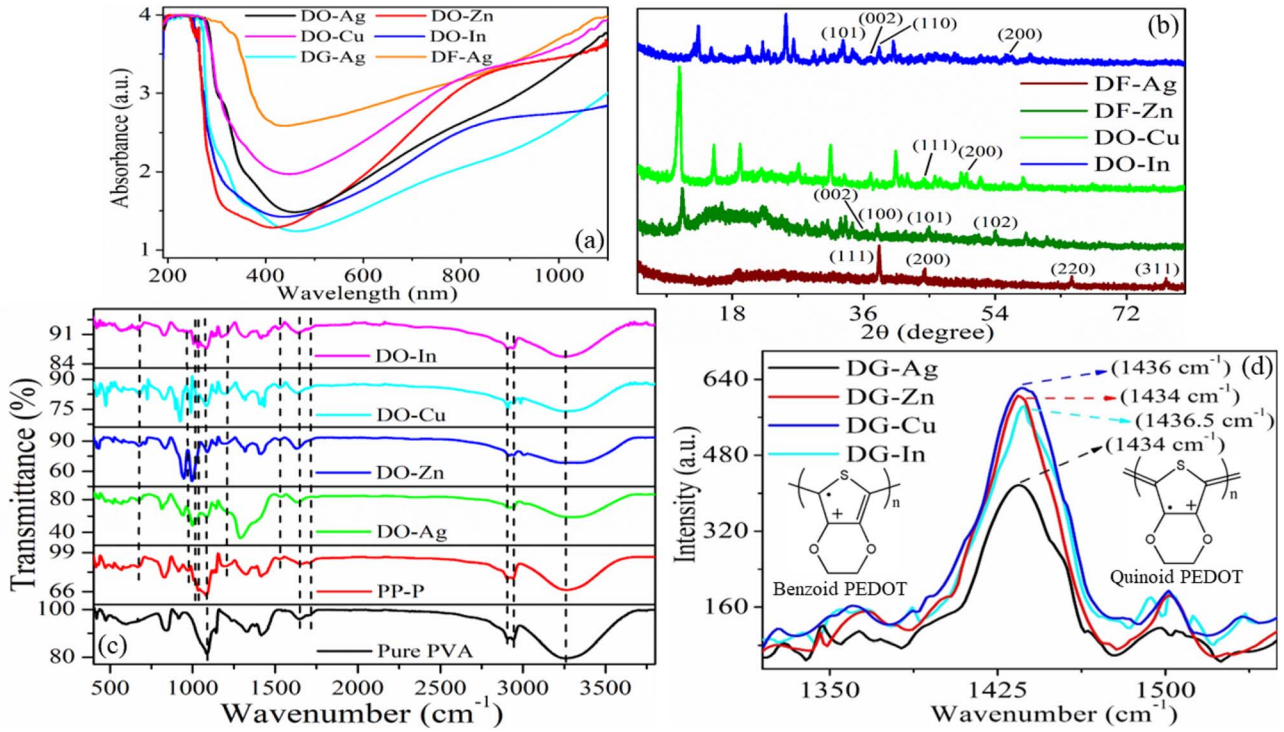

Fig. 2 (a) UV-visible spectra of the selected films, (b) XRD patterns of specified films, (c) FTIR spectra of the selected films and (d) Raman spectra of the specified films and insets represent benzoid and quinoid structures of PEDOT.

helps to grow PEDOT conductive domains.[38,43,47,48] It is also well prominent that all the films are almost blocked at near UV, far visible and near IR regions compared to far UV and near visible regions.

3.3. XRD analysis

XRD data as presented in Fig. 2(b) are taken to investigate the crystalline state and the lattice spacing between crystallographic planes as well as aggregated structure of the blended films. Here, XRD patterns are displayed for DF-Ag, DF-Zn, DO-Cu and DO-In films. For obtaining the inter-planar spacing (d), Bragg's law is employed which is written below:

$$2d \sin\theta = n\lambda \quad (1)$$

where θ, n and λ signify the incident angle, the order of diffraction and the incident X-ray wavelength respectively.[38] It is well known that pure PVA which exhibits semi-crystalline nature, has characteristic diffraction peaks at $2\theta \approx 11.3°$, 19.5°, 22.5° and 40.5° ascribing to (100), (101), (200) and (202) reflection planes respectively due to the presence of hydroxyl groups in PVA molecules and the intra- and inter-molecular hydrogen bonding between PVA chains.[46,49] It is well established that the characteristic diffraction peaks of PEDOT:PSS occur at $2\theta \approx 18.4°$ and 26° caused by π–π stacking of benzene rings of PSS and π–π stacking of thiophene rings of PEDOT respectively.[50] The sharp crystalline peaks for DF-Ag film are observed at 38.1° (d = 2.36 Å), 44.3° (d = 2.04 Å), 64.5° (d = 1.44 Å) and 77.4° (d = 1.23 Å) owing to (111), (200), (220) and (311) reflection planes of the face-centered cubic (fcc) phase of silver respectively.[51,52] The crystallite size is estimated using the Debye–Scherrer equation:

$$D = \frac{0.94 \times \lambda}{\beta \times \cos\theta} \quad (2)$$

where λ = 1.54 Å is the wavelength of Cu K_α X-ray, β represents full width at half maximum (FWHM) intensity of the peak, D is the crystallite size and θ is the diffraction angle.[46,53] The calculated crystallite sizes of DF-Ag film from 38.1°, 44.3°, 64.5° and 77.4° peaks are 38.06, 33.88, 32.06 and 32.26 nm respectively. For DF-Zn film, diffraction peaks observed at 36.3° (d = 2.47 Å), 37.9° (d = 2.37 Å), 44.8° (d = 2.02 Å) and 54.1° (d = 1.69 Å) are caused from (002), (100), (101) and (102) reflection planes respectively of zinc phase, and some other diffraction peaks are also emerged corresponding to the agglomerations of zinc chloride.[54–57] For DO-Cu film, diffraction peaks are observed at 44.3° (d = 2.04 Å) and 50.0° (d = 1.82 Å) due to the reflection planes of (111) and (200) respectively of cubic phase of fcc structure of copper, and owing to the agglomerations formed by copper chloride, some other XRD peaks are also visible.[58–63] Similarly, for DO-In film, XRD peaks become evident at 33.2° (d = 2.70 Å), 36.9° (d = 2.43 Å), 38.1° (d = 2.36 Å) and 55.8° (d = 1.65 Å) from the reflection planes of (101), (002), (110) and (200) respectively of indium, and some other peaks are also evolved which are attributed to the agglomerations of indium chloride salt.[64–67] Salt agglomerated XRD peak positions and the corresponding inter-planar spacings are displayed in Table S1 (ESI†). XRD data for DG-Ag, DG-Zn, DG-Cu and DG-In films are

presented in Fig. S2 (ESI†) and these films have almost similar type peaks as described above. It is observed that characteristic peaks of PVA, PEDOT and PSS are not appeared due to the positional disorder of these molecules caused by the higher content of used salts and also due to the effect of different interactions among constituent molecules. Such interactions and higher content of salts disrupt the continuation of longer polymer chains.[31,68] However, presence of salt makes the films relatively crystalline in nature. It is also well evidenced that characteristic diffraction peaks of PVA are almost disappeared indicating semicrystalline to amorphous transformation of PVA and the formation of disordered polymeric regions.

3.4. FTIR spectroscopy

FTIR spectra as exhibited in Fig. 2(c) are utilized for the establishment of interactions among different chemical components of the composite films and these interactions induce changes in vibrational modes at atomic or molecular levels of the materials. Pure PVA has exhibited a broad absorption peak from 2982 to 3698 cm^{-1} centred at around 3259 cm^{-1}, which is attributed to symmetric stretching vibrations of –OH groups residing in PVA by forming intramolecular and intermolecular self-associating hydrogen bonds.[10] Other peaks of pure PVA are located at 2942 and 2909 cm^{-1} (C–H stretching vibration of alkyl groups of PVA chains), 1713 cm^{-1} (C=O stretching), 1645 cm^{-1} (adsorbed water) and 1086 cm^{-1} (–C–O stretching vibration).[24–26,32,33,69] The –C=O and –C–O stretching vibrations are present as the residual acetate groups stay in PVA during its preparation through hydrolysis process from vinyl acetate.[38] After incorporation of PEDOT:PSS, *i.e.*, PP-P film, peaks caused by PEDOT are emerged at around 1525, 1203, and 973 and 667 cm^{-1} representing to stretching vibration of C=C of thiophene ring, C–O – C stretching vibration and C–S stretching vibration respectively, whereas peaks due to PSS located at 1007 and 1034 cm^{-1} represent stretching vibration of sulfonic acid group.[24,26,32,33] All other peaks of PP-P film are caused by PVA. Peaks of pure PVA and PP-P films are also presented in Table S2 (ESI†). For PP-P film, hydroxyl peak shifts to higher wavenumbers compared to pure PVA indicating the intermolecular hydrogen bond interaction of hydroxyl groups of PVA with sulfonic acid groups ($SO_3^-H^+$) of PSS. However, formation of hydrogen bonds helps to better miscibility of two components by reducing intra- and inter-molecular hydrogen bonds among PVA molecules.[10,24] For DO-Ag, DO-Zn, DO-Cu and DO-In films, hydroxyl peak further shifts to higher wavenumbers, which confirms the interaction of hydroxyl groups of PVA with sulfonic acid groups ($SO_3^-H^+$) of PSS, residual DMSO molecules and salt cations.[31,32,37,68,70] In presence of salt, it is also observed that the peak at 1203 cm^{-1} of C–O – C stretching vibration shifts to lower wavenumbers and the peak at 973 cm^{-1} of C–S stretching vibration shifts to higher wavenumbers indicating the interaction between $PEDOT^+$ and salt anions. Two PSS peaks, *i.e.*, 1007 and 1034 cm^{-1} are disappeared in presence of Ag^+ and Zn^{2+} ions indicating strong interaction of PSS sulfonic acid groups with Ag^+/Zn^{2+} ions and PVA, whereas intensity of these two peaks decreases in presence of Cu^{2+} and In^{3+} ions, which indicates relatively less interaction of PSS sulfonic acid groups with Cu^{2+}/In^{3+} ions and PVA. DG-Ag, DG-Cu and DF-Ag films have similar kinds of FTIR spectra which are presented in Fig. S3 (ESI†).

3.5. Raman spectroscopy

To find out the reason behind the conductivity enhancement in a molecular level, Raman spectroscopy was performed and presented in Fig. 2(d). In the previous study, PP-P film showed absorption peak at 1440 cm^{-1}, which was assigned to symmetric stretching vibration of C_α=C_β arising from five-membered thiophene ring of PEDOT segments.[37] DG-Ag, DG-Zn, DG-Cu and DG-In films exhibit Raman absorption peaks at 1434, 1434, 1436 and 1436.5 cm^{-1} respectively. Therefore, in presence of solvent DEG and salt, Raman peak of PP-P film shifts to lower wavenumber, *i.e.*, red-shift occurs. This red-shift represents the conversion of PEDOT conformation from benzoid to quinoid, *i.e.*, C_α=C_β bond of PEDOT transforms into C_α–C_β bond.[19,25] It is also reported that PEDOT chain exists in both benzoid and quinoid structure simultaneously. Benzoid structure looks coil-like conformation and therefore, the planes of thiophene rings deviate highly from each other. Two nearby thiophene rings are connected by C_α–C_α bond (considered as σ bond) and therefore, it has lower density of conjugated π-electrons. These, conjugated π-electrons become unable to delocalize completely along the PEDOT chains. Whereas, quinoid structure looks expanded-coil or linear-like conformation and the orientation of two adjacent thiophene rings remains almost in the same plane which completely helps to delocalize conjugated π-electrons along the whole PEDOT chains. Due to this reason, quinoid conformation improves the mobility of charge carriers in PEDOT chains and hence, enhances the conductivity.[8,26]

3.6. Surface analysis

Surface topography images as obtained from AFM are displayed in Fig. 3, which is conducive to determine surface morphology and surface roughness of the films. Surface roughness (root-mean-square roughness) for DO-Ag, DO-Zn, DO-Cu, DO-In, DG-Ag, DG-Cu, DF-Ag and DF-Cu films are obtained as ≈1.75, 0.73, 2.61, 7.69, 1.84, 11.74, 5.13 and 24.04 nm respectively. The rms roughness of PP-P film was 1.65 nm as reported in our previous study.[37] Therefore, compared to PEDOT:PSS/PVA film, *i.e.*, PP-P film, surface roughness of DO-Ag and DG-Ag films is slightly higher, whereas surface roughness of DO-Cu, DO-In, DG-Cu, DF-Ag and DF-Cu films is increased drastically. It is also observed that only for DO-Zn film surface roughness is decreased. In our previous study, PP-P film showed grains-like morphology due to the formation of hydrogen bond between PSS and PVA, whereas for PEDOT:PSS/PVA/DMSO and PEDOT:PSS/PVA/DEG films, *i.e.*, DO and DG films, stones- or rocks-like morphology was observed due to the formation of hydrogen bonds among PSS, PVA and residual solvent DMSO/DEG.[37] For PEDOT:PSS/PVA/DMF films, *i.e.*, DF films, grains-like morphology was emerged due to the hydrogen bond formation among PSS, PVA and residual solvent DMF.[38] However, after blending salts with PEDOT:PSS/PVA/solvent,

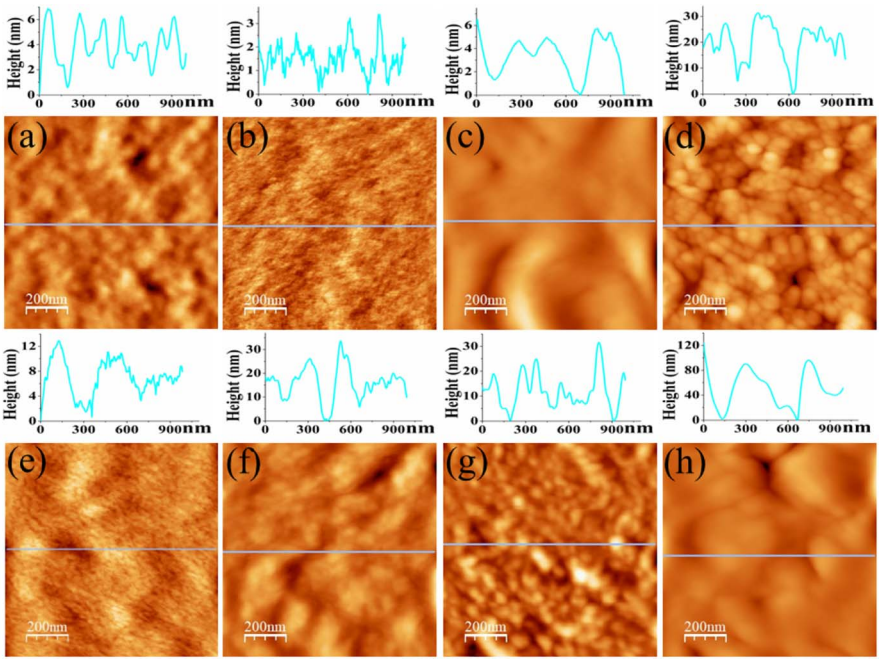

Fig. 3 AFM topography images for (a) DO-Ag, (b) DO-Zn, (c) DO-Cu, (d) DO-In, (e) DG-Ag, (f) DG-Cu, (g) DF-Ag and (h) DF-Cu films. Scanning area is $1 \times 1\ \mu m^2$.

there is again a change in surface morphology. In topography images, DO-Ag, DO-Zn, DG-Ag and DF-Ag films show comparatively smoother surfaces and have smaller grains in size attributing to comparatively good miscibility of salts with polymers throughout the whole film. Here, smaller grains are predominately formed by the combined interaction among PSS, PVA, residual solvent and salt cations and apart from that, few smaller grains are formed which may be due to the salt agglomerations. DO-Cu, DO-In, DG-Cu and DF-Cu films exhibit rougher surfaces due to the improper miscibility of salts and therefore, bigger and irregular structures are formed through the interaction among PSS, PVA, residual solvent and salt cations, which are observed along with irregularly distributed salt agglomerations. SEM images are also captured at different magnifications for the investigation of surface morphology/microstructures of PP-P, DO, DG, DF and salts mixed films, which are presented in Fig. 4. It is observed that PP-P film in Fig. 4(a) has completely smooth surface and the surface remains almost smooth even after blending 7 wt% DMSO with PEDOT:PSS/PVA, *i.e.*, DO film in Fig. 4(b). The SEM image of DO-Ag film taking at very lower magnification shows good miscibility of silver salt inside polymers and as a result mostly regular distribution of spherical morphology is formed which are observed as the brighter features in the SEM image as shown in Fig. 4(c). In addition, smaller agglomerations of silver salt are also present throughout the surface as brighter feature. DO-Zn film as depicted in Fig. 4(d) also shows almost smooth surface indicating good miscibility of zinc salt with polymers. The entire surface of DO-Cu film shown in Fig. 4(e) appears as a copper salt mixed polymeric surface along with some very small size pores, but DO-In film in Fig. 4(f) has irregular distribution of bigger and zigzag shaped morphology of bonded PSS, PVA, DMSO and In^{3+} ions along with some smaller agglomerations of indium salt. DG film surface, *i.e.*, 3 wt% DEG blended with PEDOT:PSS/PVA as shown in Fig. 4(g) is also smooth. However, DG-Ag film as presented in Fig. 4(h) shows good miscibility and at the same time regular distribution of almost square-shaped morphology of bonded PSS, PVA, DEG and Ag^{+} ions along with smaller agglomerations of silver salt is visible. Similar to DO-Cu film, copper salt mixed polymeric surface evolves with comparatively bigger pores for DG-Cu film, which is presented in Fig. 4(i). Similar to DO and DG films, DF film has completely smooth surface as shown in Fig. 4(j). However, rectangular, square and spherical-shaped morphology of bonded PSS, PVA, DMF and Ag^{+} ions become prominent for DF-Ag film along with smaller agglomerations of silver salt, which is observed in Fig. 4(k). As compared to DO-Cu and DG-Cu films, DF-Cu film depicted in Fig. 4(l) has comparatively bigger pores. From the surface analysis, it can be concluded that aggregated structures are formed as a combined interactions among PVA, salt cations, residual solvent and PSS. Apart from that, some crystalline aggregates of salt are formed on the surface of salt-blended films appearing like salt crystals, which are evidenced from the XRD analysis, and due to which AFM images exhibit dramatic increase in surface roughness.[2,21,32,71]

3.7. Mechanical studies

The typical stress–strain plots obtained from salt blended films are represented in Fig. 5(a), whereas the tensile parameters for the films such as elongation at break (%), tensile strength and toughness are plotted in Fig. 5(b). It is obvious that silver salt

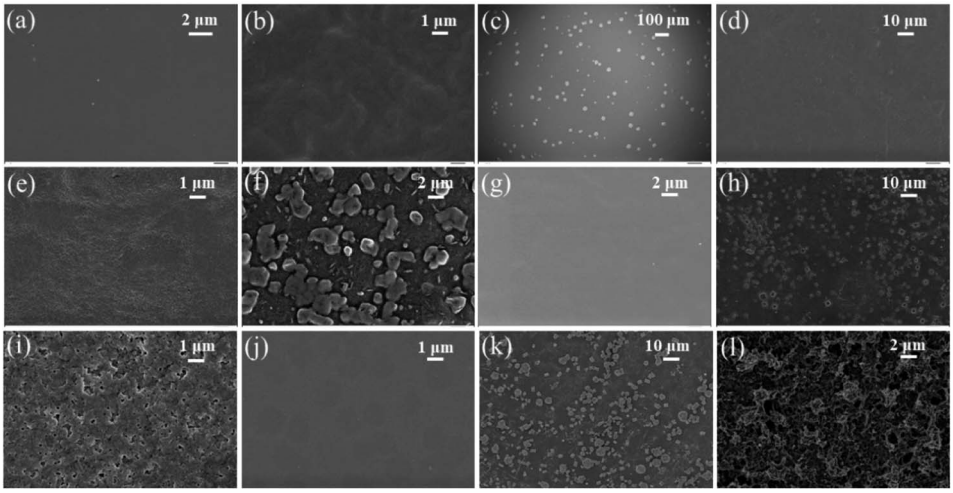

Fig. 4 SEM images for (a) PP-P, (b) DO, (c) DO-Ag, (d) DO-Zn, (e) DO-Cu, (f) DO-In, (g) DG, (h) DG-Ag, (i) DG-Cu, (j) DF, (k) DF-Ag and (l) DF-Cu films.

blended solvent films, *i.e.*, DO-Ag, DG-Ag and DF-Ag films have higher elongation at break (%) as well as toughness as compared to the other films. Elongations at break (%) for DO-Ag, DG-Ag and DF-Ag films are obtained as 670 ± 31, 592 ± 14 and 566 ± 51% respectively with the corresponding toughness values of 28.4 ± 0.9, 24.3 ± 2.2 and 23.1 ± 5.3 MPa respectively. DO-Zn film also shows good elongation at break (%) and toughness as 517 ± 15% and 8.0 ± 0.8 MPa respectively, whereas DF-Cu film shows 265 ± 45% and 13 ± 3.9 MPa respectively. Therefore, these films have large mechanical deformation, *i.e.*, highly stretchable and flexible as compared to the other films. Higher toughness is attributed to highly ductile nature of these films caused by mainly salt and residual solvent. Under high mechanical stress, DO-Ag, DG-Ag, DF-Ag, DO-Cu

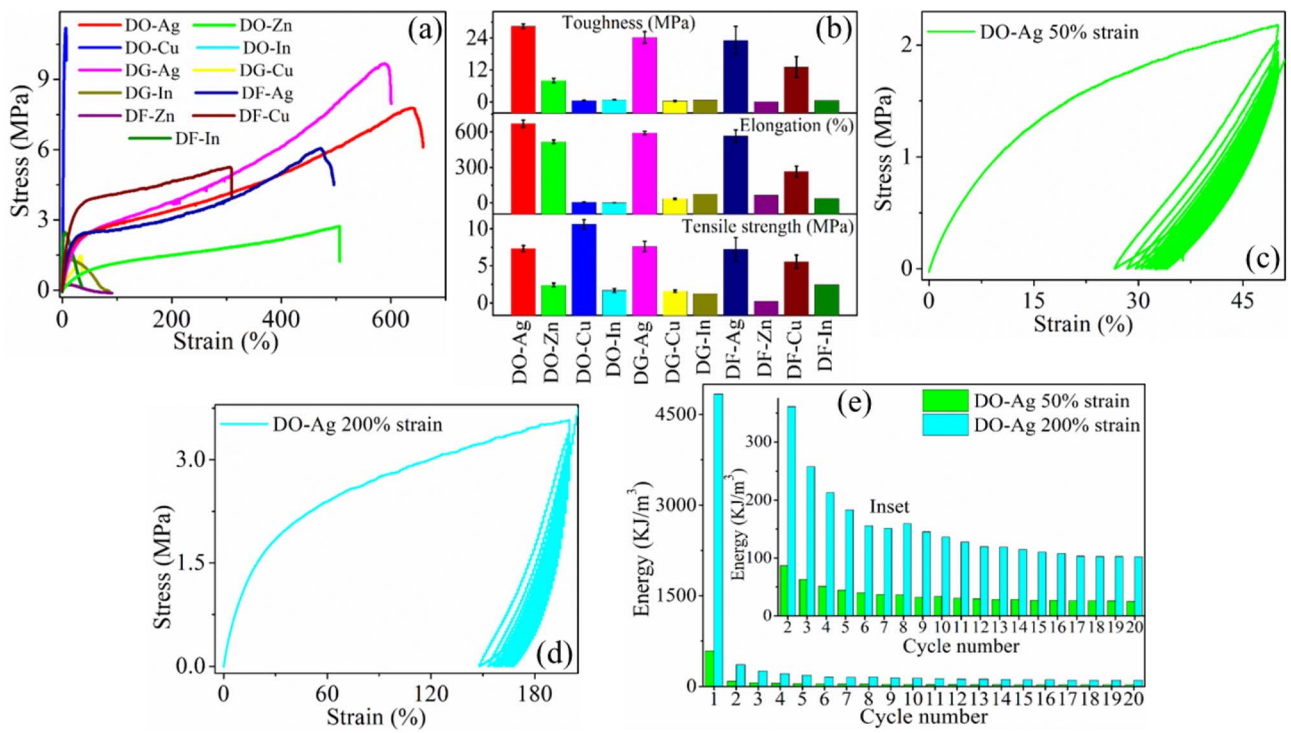

Fig. 5 (a) Typical stress–strain plots of the films. (b) The plots of different mechanical parameters such as elongation at break (%), tensile strength and toughness, (c) and (d) represent loading–unloading plots for twenty consecutive cycles at 50 and 200% strains for DO-Ag film respectively and (e) hysteresis energy plot from first to twentieth consecutive cycle at 50 and 200% strains for DO-Ag film whereas inset represents zoom version of hysteresis energy from second to twentieth cycle.

and DF-Cu films have resistance to fracture as they have higher tensile strength of 7.3 ± 0.40, 7.6 ± 0.70, 7.2 ± 1.59, 10.6 ± 0.64 and 5.6 ± 0.89 MPa respectively. In the previous studies, DO, DG and DF films, *i.e.*, 7 wt% DMSO, 3 wt% DEG and 10 wt% DMF blended PEDOT:PSS/PVA films showed elongation at break (%) as 447.0, 551.0 and 333.0 ± 17% respectively, whereas the corresponding tensile strength values were 3.2, 11.1 and 31.5 ± 1.3 MPa.[37,38] Therefore, it is obvious that presence of silver salt induces more ductilization. Therefore, DO-Ag film has optimum elongation at break (%) and toughness, whereas tensile strength is optimum for DO-Cu film. In presence of silver salt, smaller grains are regularly evolved indicating the good miscibility of silver salt with polymers by forming hydrogen bonds and ionic interactions among PSS, PVA, residual solvent and Ag^{+} ions and thus, silver salt and solvent blended films become highly ductile. At the same time, higher toughness of these films is associated with the higher plastic regions. The higher values of tensile strength for DO-Ag, DG-Ag and DF-Ag films are attributed to regularly distribution of morphology, whereas higher tensile strength for DO-Cu and DF-Cu films are ascribed to the improper miscibility of copper salts leading to the formation of bigger and irregular agglomerated-like structures formed by the interaction among PSS, PVA, residual solvent and Cu^{2+} cations along with irregularly distributed agglomerations of copper salt. For the sake of stability and durability of devices, higher tensile strength as well as higher elongation at break (%) are essential conditions for the utilization in different practical purposes such as stretchable electronics and therefore, devices can function properly for longer time without any damage risk from the mechanical force and other external energy during operation, handling and transferring.[6]

Loading–unloading experiments are performed for twenty consecutive cycles at 50 and 200% strain for some of the films, *i.e.*, for DO-Ag film at 50 and 200%, DO-Zn film at 50 and 200%, DG-Ag film at 50 and 200%, DF-Ag film at 50 and 200% and DF-Cu film at 50%. Fig. 5(c) and (d) represent loading–unloading experiments at 50 and 200% strain for DO-Ag film. The energy dissipation from first cycle to twentieth cycle at 50 and 200% strain for DO-Ag film is plotted in Fig. 5(e), whereas from second to twentieth cycle is plotted in inset of Fig. 5(e). It is obvious that energy dissipation due to the formation of hysteresis loops for the first cycle of DO-Ag film at 50 and 200% are 590.5 and 4838.4 kJ m^{-3} respectively, which is large. Energy dissipation decreases with the number of cycle and ultimately it becomes almost similar after certain number of cycles, *i.e.*, hysteresis loops overlap upon one another. The constant hysteresis behaviour for DO-Ag film at 50 and 200% is observed after 15th and 17th number of cycle. The overlapping/collapsing of hysteresis loop happens due to irreversible damage of the film network structure. Loading–unloading plots for twenty consecutive cycles at 50 and 200% strains for DO-Zn, DG-Ag and DF-Ag films, while at 50% strain for DF-Cu film are presented in Fig. S4(a)–(g) (ESI†) and hysteresis energies up to twentieth cycle are displayed in Table S3 (ESI†). All the other films exhibit huge hysteresis energy at its first cycle. At 50% strain, constant hysteresis or collapsing nature becomes obvious after 14th, 17th, 16th and 18th cycle for DO-Zn, DG-Ag, DF-Ag and DF-Cu films respectively. At 200% strain, all three DO-Zn, DG-Ag and DF-Ag films show constant hysteresis or collapsing nature after 15th cycle. At 50% strain for the first cycle, DO-Ag, DO-Zn, DG-Ag, DF-Ag and DF-Cu films can recover 23.4, 30.1, 34.9, 28.2 and 17.9% strain respectively, whereas after the completion of twentieth cycle, the corresponding films can recover 15.9, 22.8, 24.5, 17.6 and 7.9% strain. At 200% strain for the first cycle, DO-Ag, DO-Zn, DG-Ag and DF-Ag films can recover 52, 46, 86 and 20% strain respectively, whereas after the completion of twentieth cycle, the corresponding films can recover 32.1, 28.0, 64.0 and 8.0% strain. At 200% strain, *i.e.*, at higher plastic region, strain recovery is very less. The energy dissipation in the form of heat mostly occurs during loading–unloading cycles, which make all the films viscoelastic.

3.8. Electrical performance

The current (I)–voltage (V) responses of the films are displayed in Fig. 6(a) and (b). The electrical conductivities of all the films are calculated and presented in Fig. 6(c). It is clear that all the films have linear I–V characteristics. The in-plane conductivity is enunciated through the following equation.[37]

$$\sigma = \frac{\ln 2}{\pi d}\left(\frac{I}{V}\right) \quad (3)$$

where, d is thickness of the film, σ represents the conductivity, V indicates the applied voltage across the film and I is the current through the film. The average conductivities of the films remain in the range from 1.222×10^{-5} to 0.041 S cm^{-1}. Among all the films, zinc salt blended three films, *i.e.*, DO-Zn, DG-Zn and DF-Zn films have comparatively higher conductivities and DG-Zn has highest conductivity, *i.e.*, 0.041 ± 0.0014 S cm^{-1}. It is observed that among three indium salt blended films, DG-In and DF-In films have relatively good conductivities, *i.e.*, 0.012 ± 0.0014 and 0.022 ± 0.0036 S cm^{-1} respectively. Among DO-Ag, DG-Ag and DF-Ag films, DO-Ag film has highest conductivity, *i.e.*, 0.011 ± 0.0015 S cm^{-1}, whereas among all three copper salt films, DF-Cu film has highest conductivity ($4.523 \pm 1.0887 \times 10^{-5}$ S cm^{-1}). However, in our previous studies, PEDOT:PSS/PVA (PP-P) and also PEDOT:PSS/PVA in presence of solvents like DMSO, DEG and DMF, *i.e.*, DO, DG and DF films have exhibited non-linear I–V characteristics in the range of −10 to +10 V following Poole–Frenkel charge transport mechanism. Poole–Frenkel mechanism is considered as the enhancement of charge carriers released from the traps at higher electric field by decreasing the barrier height of traps, where impurity or structural defects act as traps.[37,38] The non-linear I–V characteristics in the range of −1 to +1 V for PP-P, DO, DG and DF films are shown in Fig. S5 (ESI†). Thus, non-linear to linear I–V characteristics is observed in presence of the salts.

Thus, from all the characterizations, it is clear that there are several interactions occurring in salt-blended PEDOT:PSS/PVA system in presence of solvents (DMSO, DEG and DMF) such as ionic interaction between negatively charged salt anions and positively charged $PEDOT^{+}$, ionic interaction between positively charged salt cations and negatively charged PSS^{-}, interaction

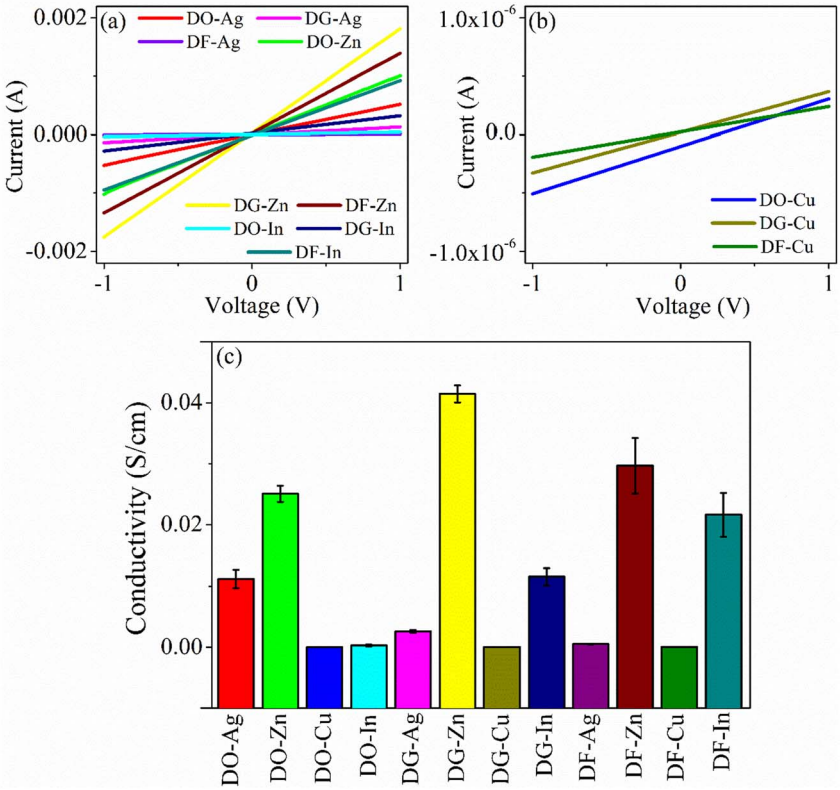

Fig. 6 (a) and (b) Typical *I–V* plots as obtained from the films and (c) electrical conductivity plot for all the films.

between salt cations and hydroxyl groups of PVA, hydrogen bond interaction between hydroxyl groups of PVA and sulfonic acid groups (–SO_3H) of PSS and also hydrogen bond interaction of residual solvent with PVA and PSS. Fig. 7(a) and (b) are schematic representations of interaction among PEDOT:PSSs and interaction among PVAs respectively. Fig. 7(c) is the existence of different possibilities of monovalent salt inside polymer medium. Fig. 7(d) is schematic representation of the possible interactions inside as prepared salt blended films. It is observed that the presence of $AgNO_3$ salt in PEDOT:PSS/PVA/solvent enhances the ductility of the films significantly compared to PEDOT:PSS/PVA/solvent films and elongation at break (%) becomes optimum for DO-Ag film. Morphological images also confirm that the silver salt blended films have lower surface roughness as well as regularly distribution of morphological features are formed by the interactions among PSS, PVA, residual solvent and Ag^+ ions. Due to the presence of such interactions, the stretchable nature of the films becomes feasible as weakly bonded or coupled system is formed and therefore, PSS and PVA chains can easily align during tensile experiment. The probable film condition in molecular level during tensile testing is schematically displayed in Fig. 7(e). From the *I–V* characteristics, it is clear that the presence of salts switches the electrical behaviour from non-linear to linear. Among all the used salts, zinc salt blended films, *i.e.*, DO-Zn, DG-Zn and DF-Zn films have optimum conductivities, while DG-Zn film shows highest conductivity, *i.e.*, 0.041 ± 0.0014 S cm^{-1}. The observed conductivities of as prepared PEDOT:PSS blended films depend on the softness parameters of the metal ions. The softness parameter values of cations of salts represent the association of the metal ions with PSS anions of PEDOT:PSS.[47] The binding energy of the metal ions with other ions relies on the softness parameter of the specific metal ion. The inorganic cations such as Zn^{2+}, In^{3+}, Ag^+ and Cu^{2+} have positive softness parameters which are +0.35, +0.48, +0.18 and +0.38 respectively and therefore, their salts are able to elevate the conductivity of the PEDOT:PSS film significantly. Whereas the inorganic cations of negative softness parameters are less effective to elevate the conductivity of the PEDOT:PSS film.[34,35] Cations having a positive (or negative) softness parameter are considered as soft (or hard) Lewis acid. According to the hard and soft acid and base (HSAB) concept, a hard acid with a hard base and a soft acid with a soft base are interacted strongly. For $ZnCl_2$, as an example, Zn^{2+} cations interact with PSS^- anions and Cl^- anions interact as a counterions with $PEDOT^+$ cations, which promotes the formation of conductive domains/pathways *via* π–π stacking of PEDOT chains by decoupling of PEDOT from PSS. This process also leads to the PEDOT conformation change from coil-like to expanded-coil or linear-like. Here, the delocalization of positive charge of PEDOT generally happens after some monomer units *via* π conjugation, whereas the localization of the negative charge of the chloride anions exists highly at the atomic level. Therefore, interaction between $PEDOT^+$ and Cl^- would be regarded as soft acid and hard base interaction, which makes Cl^- ions easily detachable. Therefore, strong interaction between PSS^- and Zn^{2+} and relatively weak

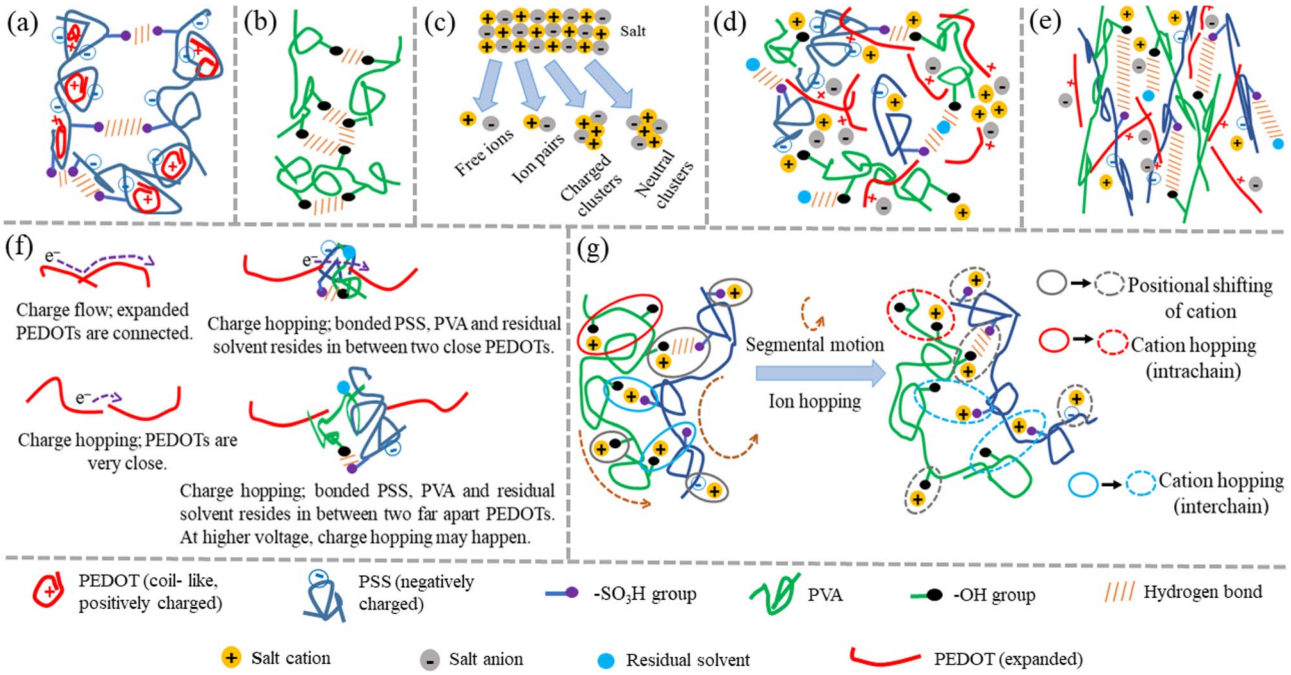

Fig. 7 Probable schematic representations. (a) Interaction among PEDOT:PSSs, (b) interaction among PVAs, (c) existence of different possibilities of monovalent salt inside polymer medium, (d) possible interactions inside as prepared salt blended films, (e) salt blended film condition in molecular level during tensile testing, (f) electronic conduction mechanism of PP-P, DO, DG and DF films and (g) segmental motion and ion hopping of salt blended films.

interaction between $PEDOT^+$ and Cl^- occurs. The ion-interaction mechanism of PEDOT material significantly enhances the mobility of electrons, while their density slightly reduces.[6,36,45,47,72,73] Two interconnected parameters, *i.e.*, ion concentration and ion mobility govern the ionic conductivity. Mobile ion concentration depends on salt concentration and the ability of salt dissociation by solid polymer electrolytes (SPEs). Salt ions (monovalent) inside SPEs reside in equilibrium and can stay as free ions (charged and dissociated ions), ion pairs (neutral and associated ions) and ionic clusters (comprising of >2 ions, charged or neutral) shown in Fig. 7(c). Whereas multivalent salt ions inside electrolyte reside in a little complex way and have larger ionic clusters.[74,75] For associated ions, their motion solely depends on the lifetime of the ion-association, which influences both the ion-migration and the flux of charge. For the description of whole population of aggregates, many equilibrium systems have to be considered. For the sake of simplicity, this complex equilibrium system is considered as a single equilibrium system between ion pairs and dissociated ions indicated by the extent of ion-dissociation (ξ) (sometimes also regarded as ionicity).

$$\xi = \frac{[\text{Free ions}]}{[\text{Total ions}]} \tag{4}$$

The ion dissociation extent ξ is driven as a function of two parameters, *i.e.*, the identity of ionic species and the properties of the background medium such as ion–electrolyte interactions and dielectric properties of the medium. The dissociated ions generate due to the solvation of salts into the electrolyte by salt-doping. High conductivity is achieved for high extent of ion dissociation. ξ depends on both the host polymer and salt identity.[74] The ionic conductivity (σ) is attributed to the motion of net charge arising from all dissociated ions and clusters.

$$\sigma = \sum ec_n|z_n|^2\mu_n \tag{5}$$

where e dictates the elementary charge, μ_n represents the specific mobility, c_n is called concentration and z_n indicates the charge of cluster 'n'. For neutral ion pairs, $z_n = 0$ as they do not play any role to ionic conductivity.[74–76] Therefore, two terms (*i.e.*, dissociated cations and anions) remain in the below equation under simplified equilibrium condition.

$$\sigma = ec_{\text{salt}}\xi(|z_+|^2\mu_+ + |z_-|^2\mu_-) \tag{6}$$

The cation transport number t_+ is enunciated through self-diffusion coefficients comprising of all mobile ionic species/clusters in the electrolyte.[74,77]

$$t_+ = \frac{|Z_+|^2\mu_+}{|Z_+|^2\mu_+ + |Z_-|^2\mu_-} \tag{7}$$

Ion dynamics inside polymeric material does not follow the simplified diffusion of liquid. The transportation of ions in SPEs is mainly governed by a combined effect of segmental motion, ion-hopping and vehicle mechanism. Above the glass transition temperature (T_g), the segmental mobility of polymer backbone or side chains often occur in the amorphous regions

of polymer. The cation transport through polymer chains happens if the coordination of cations exists with highly electron donor polar groups of polymers. These polar groups are beneficial for the dissociation of salts. The dissociation of inorganic salt in polymer system becomes more feasible through the reduction of lattice energy of salt and elevating the dielectric constant of the polymer.[75,76,78–80] Here, after incorporation of salts, it is obvious from XRD that polymeric regions of PVA transform from semicrystalline to almost amorphous nature, whereas PSS regions remain in amorphous state and therefore, the prepared polymeric films show flexibility. Thus, segmental motion is occurred inside polymer chains. As the cations of salt are coordinated with the polar groups of PEDOT:PSS (*i.e.* $-SO_3^-$, $-SO_3H$ and –S groups) and PVA (*i.e.* –OH groups), migration of cations through segmental motion of PVA and PSS backbone or side chains occurs. As PEDOT is rigid, segmental motion of PEDOT chains is almost impossible and therefore, migration of salt cations through PEDOT chains is not occurred. At the same time, anions of salts which are interacting with PEDOT, are unable to migrate. Compared to inorganic electrolytes, the interaction between polymer and cation is strong and the mean free path for ion hopping is also large. Apart from the independent ion-hopping in polymer, ion-hopping may also accompany with segmental motion of polymer chains. Ultimately, ion jumps from one polymer chain to another. Both intra- and inter-chain ion-hopping are also possible. Ion motion though the vehicle mechanism is generally occurred in liquids, where ions are driven by the free diffusion of charge carriers. The vehicle mechanism promotes the transport of protons.[74,76,80,81] However, for PEDOT:PSS/PVA (PP-P) and also PEDOT:PSS/PVA/solvents like DMSO, DEG and DMF, *i.e.*, DO, DG and DF films, hydrogen bonds among PSS, PVA and residual solvent are beneficial for the separation of $PEDOT^+$ from PSS^- and therefore, PEDOT changes its conformation from coil-like to expanded-coil or linear-like, which helps to connect or close PEDOT chains with other ones. At the same time, many non-conducting regions owing to the hydrogen bonds among PSS, PVA and residual solvent act like traps for charge carries. These non-conducting regions reside throughout the film and of course, some of them stay in between elongated PEDOT chains. Therefore, conducting pathways are formed in four ways, *i.e.*, continuous electron flow along the whole elongated PEDOT backbone *via* overlapping of π-orbitals as well as continuous electron flow between directly connected PEDOTs *via* overlapping of adjacent π-orbitals, electron hopping from the π-orbital of one PEDOT polymer chain to other when PEDOTs are very close apart, electron hopping when bonded PSS, PVA and residual solvent resides in between two close PEDOTs and also electron hopping when bonded PSS, PVA and residual solvent resides in between two far away PEDOTs, which are schematically presented in Fig. 7(f). At higher voltage, decrement of barrier height of traps occurs, which enhances the release of charge carries from the traps though Poole–Frenkel mechanism. Therefore, for PP-P, DO, DG and DF films, non-linear current responses are observed.[37,38,81] However, the presence of salt in PEDOT:PSS/PVA/solvent generates more and more elongated PEDOT chains and therefore, more conducting pathways are formed due to the connection of elongated PEDOT–PEDOT chains. From SEM and AFM images, it is observed that the introduction of salts promotes to evolve some different shaped morphologies due to the interaction among PVA, salt cation, residual solvent and PSS counterparts along with some agglomerations of salts appearing like salt crystals. Here, bonded PVA, salt cation, residual solvent and PSS counterparts are conducting as the movement of dissociated salt cations through segmental motion of PVA and PSS chains along with the hopping (intra- and inter-chain) of salt cations occur, which is schematically displayed in Fig. 7(g). As schematically shown, ionic conduction generally occurs in two different ways: electrostatic interaction with electron withdrawing moieties in the polymer side chains, and due to the movement of the polymer segments, for which free-volume sites are created. When free-volume sites are closed, ions can hop from one site to other.[75,81,82] These bonded conducting counterparts reside throughout the film, *i.e.*, some of them stay in between elongated PEDOT chains and others stay in the outside regions. Apart from that, salt agglomerations are created, which form crystalline domains. Some salt agglomerations act as charged ionic clusters and also contribute to ionic conduction staying separately or in between elongated PEDOT chains.[32,83] Therefore, due to salt addition, more and more short or long-range conducting pathways are created and as a result charge transport follows linear behaviour instead of non-linearity. From FTIR, UV-visible, AFM and SEM results, it is also concluded that zinc salt blended films have better conductivity compared to others like silver, copper and indium salts, which is due to the lower surface roughness as well as good miscibility of zinc salt (*i.e.* excellent salt dissociation) in the polymer system and therefore, more dissociated ions generate which in turn, provides more mobile ions especially here, cations and these cations are highly beneficial for conduction mechanism through segmental motion and cation hopping. Copper salt blended films have lower conductivity due to the formation of pores and brittle nature, which obstructs the segmental motion and ion hopping and therefore, motion of salt cations is hindered. Among all the twelve films, it is found that $ZnCl_2$ blended PEDOT:PSS/PVA/DMSO film shows relatively superior behaviours having both considerable electrical conductivity (0.025 ± 0.0013 S cm^{-1}) and elongation at break ($517 \pm 15\%$) values.

4. Conclusions

In the present work, mechanically ductile and conducting films are fabricated by blending different solvents (DMSO, DEG and DMF) and salts ($AgNO_3$, $ZnCl_2$, $CuCl_2$ and $InCl_3$) with the homogeneous solution of PEDOT:PSS/PVA followed by solution casting method and room temperature drying. It is observed that presence of salts with PEDOT:PSS/PVA/solvents switches the current response from non-linear to linear. The linear behaviour arises due to the multiple reasons. The probability of interconnection of PEDOT chains enhances in presence of salt due to the conversion of PEDOT structure from benzoid to quinoid as the hydrogen bond and ionic interaction among PSS,

PVA, residual solvent and salt cations as well as the electrostatic interaction between $PEDOT^+$ and salt anions occur. Dissociated salt ions transport *via* both segmental motion of PVA and PSS polymer side chains or backbone, and ion hopping. Apart from that, salt agglomerations can grow crystalline domains that are beneficial for electrical conduction. Thereby, conducting pathways become feasible due to the transportation of electrons and ions. Among all the used salts, $ZnCl_2$ blended films, *i.e.*, DO-Zn, DG-Zn and DF-Zn films have higher conductivities due to lower surface roughness and well miscibility. DG-Zn film has highest conductivity, *i.e.*, 0.041 ± 0.0014 S cm^{-1} as compared to other films. However, the interaction among PSS, PVA, residual solvent and salt cations by reducing coulombic interaction between $PEDOT^+$ and PSS^-, and also lowering intra- and intermolecular PVA interaction is responsible for the stretchability of the films. Silver salt blended solvent films, *i.e.*, DO-Ag, DG-Ag and DF-Ag films have higher elongation at break (%) as well as toughness as compared to other films and it is attributed to lower surface roughness and regularly morphological distribution generation owing to the hydrogen bond and ionic interactions among PSS, PVA, DMSO and Ag^+ ions. Elongation at break (%) for DO-Ag film is observed maximum as $670 \pm 31\%$. However, $ZnCl_2$ blended PEDOT:PSS/PVA/DMSO film exhibits excellent behaviours considering both conductivity and elongation values. Thus, salt induced mechanically ductile and conducting free-standing films are successfully fabricated through cost-effective as well as environmentally friendly way and may be utilized in the diverse fields such as wearable devices, bioelectronics, soft robotics, *etc.*

Author contributions

S. Sau has conceptualized the work, performed all the experiments, analyzed the results and wrote the manuscript. S. Kundu supervised the work and critically reviewed and edited the manuscript. Both the authors approved the manuscript.

Conflicts of interest

The authors declare that there are no conflicts of interest.

Acknowledgements

The current work was executed by the financial assistance (INSPIRE Fellowship (IF180888) to S. Sau) from Department of Science and Technology, Govt. of India. S. Kundu confirms the financial assistance from Department of Science and Technology, Govt. of India. Both authors thank IASST, Guwahati for the financial as well as all experimental facilities.

References

1 H. He and J. Ouyang, *Acc. Mater. Res.*, 2020, **1**, 146–157.
2 M. J. Donahue, A. Sanchez-Sanchez, S. Inal, J. Qu, R. M. Owens, D. Mecerreyes, G. G. Malliaras and D. C. Martin, *Mater. Sci. Eng.*, 2020, **140**, 100546.
3 T. Le, Y. Kim and H. Yoon, *Polymers*, 2017, **9**, 150.
4 N. K and C. S. Rout, *RSC Adv.*, 2021, **11**, 5659–5697.
5 G. Kougkolos, M. Golzio, L. Laudebat, Z. Valdez-Nava and E. Flahaut, *J. Mater. Chem. B*, 2023, **11**, 2036–2062.
6 H. He, R. Chen, S. Yue, S. Yu, J. Wei and J. Ouyang, *Sci. Adv.*, 2022, **8**, 47.
7 J. Ouyang, *SmartMat*, 2021, **2**, 263–285.
8 J. Yang, Y. Jia, Y. Liu, P. Liu, Y. Wang, M. Li, F. Jiang, X. Lan and J. Xu, *Compos. Commun.*, 2021, **27**, 100855.
9 X. Strakosas, M. Sessolo, A. Hama, J. Rivnay, E. Stavrinidou, G. G. Malliaras and R. M. Owens, *J. Mater. Chem. B*, 2014, **2**, 2537–2545.
10 J. Yin, Y. Bai, J. Lu, J. Ma, Q. Zhang, W. Hong and T. Jiao, *Colloids Surf., A*, 2022, **643**, 128791.
11 A. F. Al Naim and A. G. El-Shamy, *Mater. Sci. Semicond. Process.*, 2022, **152**, 107041.
12 A. Bafekry, M. M. Fadlallah, C. Nguyen and D. Gogova, *Appl. Phys. Lett.*, 2020, **117**, 233101.
13 Y. Yu, S. Peng, P. Blanloeuil, S. Wu and C. H. Wang, *ACS Appl. Mater. Interfaces*, 2020, **12**, 36578–36588.
14 J. R. Aggas, S. Abasi, J. F. Phipps, D. A. Podstawczyk and A. Guiseppi-Elie, *Biosens. Bioelectron.*, 2020, **168**, 112568.
15 W. Zhao, B. Yalcin and M. Cakmak, *Synth. Met.*, 2015, **203**, 107–116.
16 H. Shi, C. Liu, Q. Jiang and J. Xu, *Adv. Electron. Mater.*, 2015, **1**, 1500017.
17 L. V. Kayser and D. J. Lipomi, *Adv. Mater.*, 2019, **31**, 1806133.
18 X. Fan, W. Nie, H. Tsai, N. Wang, H. Huang, Y. Cheng, R. Wen, L. Ma, F. Yan and Y. Xia, *Adv. Sci.*, 2019, **6**, 1900813.
19 Y. Yang, G. Zhao, X. Cheng, H. Deng and Q. Fu, *ACS Appl. Mater. Interfaces*, 2021, **13**, 14599–14611.
20 U. Lang, N. Naujoks and J. Dual, *Synth. Met.*, 2009, **159**, 473–479.
21 C. Chen, A. Torrents, L. Kulinsky, R. D. Nelson, M. J. Madou, L. Valdevit and J. C. LaRue, *Synth. Met.*, 2011, **161**, 2259–2267.
22 G. Massaglia, A. Chiodoni, S. L. Marasso, C. F. Pirri and M. Quaglio, *J. Nanomater.*, 2018, **2018**, 1–7.
23 S. Li, Y. Cong and J. Fu, *J. Mater. Chem. B*, 2021, **9**, 4423–4443.
24 X. Wang, G. Feng, M. Li and M. Ge, *Polym. Bull.*, 2019, **76**, 2097–2111.
25 J. Wei, C. Du, P. Li, X. Zhou, C. Zhou and S. Yang, *Sep. Purif. Technol.*, 2022, **295**, 121335.
26 X. Wang, M. Li, G. Feng and M. Ge, *Appl. Phys. A*, 2020, **126**, 184.
27 M. Bazzi, I. Shabani and J. A. Mohandesi, *J. Mech. Behav. Biomed. Mater.*, 2022, **125**, 104975.
28 R. Hemalatha, M. Alagar, S. Selvasekarapandian, B. Sundaresan, V. Moniha, G. Boopathi and P. C. Selvin, *Ionics*, 2018, **25**, 141–154.
29 Y. Liu, W. Wang, K. Gu, J. Yao, Z. Shao and X. Chen, *ACS Appl. Mater. Interfaces*, 2021, **13**, 29008–29020.
30 S. Panigrahy and B. Kandasubramanian, *Eur. Polym. J.*, 2020, **132**, 109726.
31 M. Ramaswamy, T. Malayandi, S. Subramanian, J. Srinivasalu and M. Rangaswamy, *Ionics*, 2017, **23**, 1771–1781.

32 J. Gong, F. Sun, Y. Pan, A. Fei, S. Leicheng, F. Du and Y. Zhang, *Mater. Today Commun.*, 2022, **33**, 104324.
33 Q. Gao, M. Wang, X. Kang, C. Zhu and M. Ge, *Compos. Commun.*, 2020, **17**, 134–140.
34 Y. Xia and J. Ouyang, *Macromolecules*, 2009, **42**, 4141–4147.
35 Z. Fan, D. Du, Z. Yu, P. Li, Y. Xia and J. Ouyang, *ACS Appl. Mater. Interfaces*, 2016, **8**, 23204–23211.
36 Y. Xia, H. Zhang and J. Ouyang, *J. Mater. Chem.*, 2010, **20**, 9740–9747.
37 S. Sau and S. Kundu, *Colloids Surf., A*, 2022, **636**, 128130.
38 S. Sau and S. Kundu, *Colloids Surf., A*, 2023, **664**, 131082.
39 Z. Yu, Y. Xia, D. Du and J. Ouyang, *ACS Appl. Mater. Interfaces*, 2016, **8**, 11629–11638.
40 M. O. P. Kara and M. W. Frey, *J. Appl. Polym. Sci.*, 2014, **131**, 40305.
41 A. Rianjanu, A. Kusumaatmaja, E. A. Suyono and K. Triyana, *Heliyon*, 2018, **4**, e00592.
42 K. H. Stern, *J. Phys. Chem. Ref. Data*, 1972, **1**, 747–772.
43 Y. Gan, S. Bai, S. Hu, X. Zhao and Y. Li, *RSC Adv.*, 2016, **6**, 56728–56737.
44 J. G. Raja, M. B. Ahamed, C. M. Hussain and P. Era, *J. Mater. Sci.: Mater. Electron.*, 2022, **33**, 22883–22898.
45 H. Cho, W. Cho, Y. Kim, J. Lee and J. H. Kim, *RSC Adv.*, 2018, **8**, 29044–29050.
46 S. Sau and S. Kundu, *J. Mol. Struct.*, 2022, **1250**, 131699.
47 S. Horike, Q. Wei, K. Kirihara, M. Mukaida, Y. Koshiba and K. Ishida, *J. Mater. Chem. C*, 2021, **9**, 15813–15819.
48 O. Yarema, M. Yarema, D. Bozyigit, W. M. M. Lin and V. Wood, *ACS Nano*, 2015, **9**, 11134–11142.
49 S. Sau, S. Pandit and S. Kundu, *Surf. Interfaces*, 2021, **25**, 101198.
50 L. Ouyang, C. Musumeci, M. J. Jafari, T. Ederth and O. Inganäs, *ACS Appl. Mater. Interfaces*, 2015, **7**, 19764–19773.
51 L. Tang, F. Duan and M. Chen, *RSC Adv.*, 2016, **6**, 65012–65019.
52 B. Abebe, B. Kefale and D. T. Leku, *RSC Adv.*, 2023, **13**, 4523–4529.
53 T. Saleh, A. Kösemen, S. E. San and M. K. El Mansy, *Optik*, 2014, **125**, 2009–2016.
54 N. Alias and A. A. Mohamad, *J. King Saud Univ., Eng. Sci.*, 2015, **27**, 43–48.
55 M. K. Trivedi, K. K. Sethi, P. Panda and S. Jana, *Int. J. Pharm. Invest.*, 2017, **7**, 33–40.
56 M. K. Trivedi and S. Jana, *J. adv. pharm. sci. technol.*, 2021, **2**, 11–25.
57 T. Long, S. Yin, K. Takabatake, P. Zhnag and T. Sato, *Nanoscale Res. Lett.*, 2009, **4**, 247–253.
58 S. Datta, A. S. Mahapatra, P. Sett, M. Ghosh, P. K. Mallick and P. K. Chakrabarti, *J. Sci.: Adv. Mater. Devices*, 2018, **3**, 113–121.
59 E. M. AbouElleef, M. M. Mahrouka and S. E. Salem, *Bioinorg. Chem. Appl.*, 2021, **2021**, 1–15.
60 K. Chen and D. Xue, *CrystEngComm*, 2013, **15**, 1739.
61 R. V. Singh, M. R. Pai, A. M. Banerjee, C. Nayak, S. Phapale, D. Bhattacharyya and A. K. Tripathi, *J. Therm. Anal. Calorim.*, 2021, **147**, 7063–7076.
62 G. Zhang, B. Xu, H. Chong, W. Wei, C. Wang and G. Wang, *RSC Adv.*, 2019, **9**, 14016–14023.
63 M. Fikry, W. Tawfik and M. M. Omar, *Opt. Quantum Electron.*, 2020, **52**, 249.
64 S. Gu, B. Fu, G. Dodbiba, T. Fujita and B. Fang, *RSC Adv.*, 2017, **7**, 52017–52023.
65 G. Purwiandono, K. Manseki and T. Sugiura, *RSC Adv.*, 2020, **10**, 37576–37581.
66 A. A. Naberezhnov, A. E. Sovestnov and A. V. Fokin, *Tech. Phys.*, 2011, **56**, 637–641.
67 J. J. Calvin, T. M. Kaufman, A. B. Sedlak, M. F. Crook and A. P. Alivisatos, *Nat. Commun.*, 2021, **12**, 2663.
68 M. Ramaswamy, T. Malayandi, S. Subramanian, J. Srinivasalu, M. Rangaswamy and V. Soundararajan, *Polym.-Plast. Technol. Eng.*, 2017, **56**, 992–1002.
69 A. Selim, A. J. Toth, D. Fozer, K. Suvegh and P. Mizsey, *ACS Omega*, 2020, **5**, 32373–32385.
70 P. Quan, X. Wan, Q. Tian, C. Liu and L. Fang, *J. Controlled Release*, 2020, **317**, 142–153.
71 M. Sajid, H. B. Kim, Y. J. Yang, J. Jo and K. Choi, *Sens. Actuators, B*, 2017, **246**, 809–818.
72 A. R. Hopkins and J. R. Reynolds, *Macromolecules*, 2000, **33**, 5221–5226.
73 S. Zhang, Z. Fan, X. Wang, Z. Zhang and J. Ouyang, *J. Mater. Chem. A*, 2018, **6**, 7080–7087.
74 S. D. Jones, J. Bamford, G. H. Fredrickson and R. A. Segalman, *ACS Polym. Au*, 2022, **2**, 430–448.
75 S. Hazra, A. Banerjee and A. K. Nandi, *ACS Omega*, 2022, **7**, 32849–32862.
76 S. T. Keene, V. Gueskine, M. Berggren, G. G. Malliaras, K. Tybrandt and I. Zozoulenko, *Phys. Chem. Chem. Phys.*, 2022, **24**, 19144–19163.
77 H. Xu, M. Jing, J. Li, Z. Huang, T. Wang, W. Yuan, B. Ju and X. Shen, *ACS Sustainable Chem. Eng.*, 2021, **9**, 11118–11126.
78 Y. Li, S. Park, K. Sarang, H. Mei, C. Tseng, Z. Hu, D. Zhu, X. Li, J. Lutkenhaus and R. Verduzco, *ACS Polym. Au*, 2023, **3**, 267–275.
79 K. Les and C. Jordan, *RSC Adv.*, 2020, **10**, 41296–41304.
80 H. Yang and N. Wu, *Energy Sci. Eng.*, 2022, **10**, 1643–1671.
81 J. W. Onorato and C. K. Luscombe, *Mol. Syst. Des. Eng.*, 2019, **4**, 310–324.
82 E. M. Thomas, P. H. Nguyen, S. D. Jones, M. L. Chabinyc and R. A. Segalman, *Annu. Rev. Mater. Res.*, 2021, **51**, 1–20.
83 E. M. Sheha, M. M. Nasr and M. K. El-Mansy, *J. Adv. Res.*, 2015, **6**, 563–569.